





The Relationship Between Particle-Void Fabric and Pre-liquefaction Behaviors of Granular Soils

Jiangtao Wei^(✉) , Minxuan Jiang, and Yingbin Zhang 

Southwest Jiaotong University, Chengdu, China
jtwei@swjtu.edu.cn

Abstract. When driven by undrained cyclic shearing, saturated granular soils will experience the increase of excess pore water pressure and the decrease of effective stress. This phenomenon is termed as “cyclic liquefaction” or “cyclic softening”. Revealing the evolution of fabric in accompany with effective stress reduction provides a significant insight into the fundamental mechanism of cyclic liquefaction. In this study, numerical tests were conducted in DEM simulations to explore the cyclic liquefaction of granular packings with different void ratios. With the decrease of mean effective stress p' during cyclic liquefaction process, the decrease of particle-void descriptor E_d can be observed for all packings. From the micromechanical perspective, large size voids are redistributed and the local void distribution around particle becomes relative uniform. The change of particle-void fabric from consolidated state to initial liquefaction state is irrelevant to density of the packing. A power function is further adopted to describe the negative correlation between E_d and p' .

Keywords: Discrete-element method · Cyclic liquefaction · Particle-void fabric

1 Introduction

Cyclic liquefaction of granular soils has attracted considerable interests from researchers and engineers from both geotechnical and seismic fields since 1964 Nigaata Earthquake. After initial liquefaction, granular soils will be transformed between “fluid-like” state and “solid-like” state (Idriss and Boulanger 2008; Shamoto et al. 1997; Wei et al. 2018). Granular packing in the “solid-like” state can resist external load whereas packing in the “fluid-like” state flows under any applied loads. In terms of cyclic liquefaction of a granular system, geotechnical researchers were interested in the liquefaction potential and liquefaction assessment of granular soils (Vaid et al. 2001; Idriss and Boulanger 2008; Yang and Sze 2011), and the consequences of cyclic liquefaction such as lateral spreading and post-liquefaction settlement (Ishihara 1993; Shamoto et al. 1997).

A great number of studies have revealed that cyclic liquefaction of granular soils mainly attributes to the collapse of load bearing structure, which can be reflected by the decrease of coordination number (Wang and Wei 2016; Wang et al. 2016; Sitharam et al. 2009). This is from the contact-based fabric to explain the cyclic liquefaction. However, few studies have probed cyclic liquefaction phenomenon from void-based

fabric, partially due to the difficulty to define individual void (Li and Li 2009; Ghedia and O'Sullivan 2012). Wang et al. (2016) proposed a fabric entity termed as mean neighboring particle distance (MNPD) to reflect space arrangement of particles. Wei et al. (2018) proposed fabric descriptors based on Voronoi tessellation to quantify the anisotropy of local void distribution. These studies revealed that the void-based fabric was strongly correlated with large post-liquefaction deformation of granular soils. How the void-based fabric evolves with the effective stress reduction in pre-liquefaction is not well understood.

In this study, comprehensive numerical tests were performed in DEM (discrete element method) simulations to explore the cyclic liquefaction of granular soils from void-based fabric perspective. DEM has been proven to be an excellent tool to study cyclic behaviors of granular soils (Sitharam et al. 2009; O'Sullivan 2011; Huang et al. 2018). Particle-void descriptors proposed by Wei et al. (2018) were adopted to quantify void-based fabric, in terms of particle arrangement and local void distribution within the granular packing. Evolution of particle-void descriptors in accompany with the decrease of mean effective stress in cyclic liquefaction process is further explored for samples with different densities.

2 Methodology and Approach

2.1 Numerical Setups in DEM Simulation

Numerical simulations in this study are carried out in an open-source DEM platform YADE (Smilauer et al. 2015), which has been widely used to perform DEM simulations. Granular packings in the simulation are generated in a 2D square box with the periodic boundaries in all directions. The packing consists of 4,000 frictional disks, with the radii ranges from 0.3 to 0.6 mm. The simplified Hertz-Mindlin model is employed to describe the contact behaviors between contacted particles (Yimsiri and Soga 2010; Wei and Wang 2020). In the contact model, the normal contact force is given by

$$f_n = k_n \delta \quad (1)$$

$$k_n = \frac{2E\sqrt{r}}{3(1-\nu^2)}\sqrt{\delta} \quad (2)$$

where k_n is the normal stiffness and δ is the contact overlap. r is the equivalent radius determined by the radii of two contacted particles: $r = \frac{r_A r_B}{r_A + r_B}$. E and ν are Young's modulus and Poisson's ratio of particles, respectively. In the DEM modellings, $E = 67$ GPa and $\nu = 0.3$.

The tangential contact force is given by

$$df_s = k_s dU_s \quad (3)$$

$$k_s = \frac{2E\sqrt{r}}{(1+\nu)(2-\nu)}\sqrt{\delta} \quad (4)$$

where k_s is the tangential stiffness, U_s is the tangential displacement of the contact. The tangential contact force satisfies the Coulomb criterion that $f_s < \mu f_n$, and μ is the frictional coefficient of particle. After generation of particles within a 2D square box, the packing is firstly subjected to an isotropically consolidation process to reach the confining stress $p_0 = 10 \text{ kPa}$.m. Figure 1(a) demonstrates the consolidated packing. In this process, packings with different void ratios can be obtained by assigning different frictional coefficient μ to particles. In the simulation, four samples with different void ratios (i.e. $e = 0.206, 0.214, 0.222, 0.231$) are prepared, in order to explore the influence of density to the evolution of fabric.

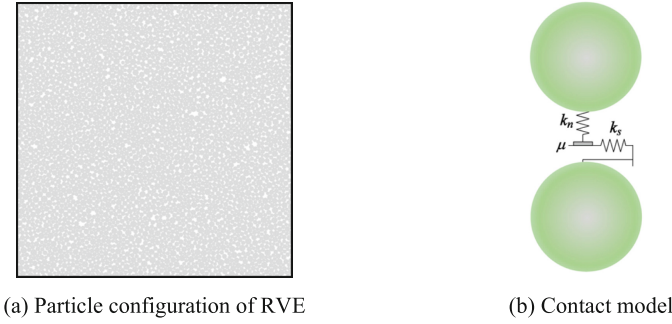


Fig. 1. Granular packing in the numerical simulation.

2.2 Quantification of Void-Based Fabric

To quantitatively explore the void-based fabric in a granular packing, we follow the approach proposed by Wei et al. (2018). In the approach, the granular packing is firstly partitioned into microscopic particle-void cells using Voronoi tessellation. As shown in Fig. 2, each cell is polygonal shape and consists of one particle and its surrounding voids. Local void distribution in the cell is further described by the function $r(\theta)$, which is defined as the ratio between the radial dimension of the cell and the particle:

$$r(\theta) = \frac{R_c(\theta)}{R_p(\theta)} \quad (5)$$

Using Fourier descriptor analysis (Bowman et al. 2001), $r(\theta)$ can be approximated by a concise expression with three parameters:

$$r^2(\theta) \approx \frac{A_r}{\pi} [1 + e_d \cos 2(\theta - \theta_d)] \quad (6)$$

where A_r is the enclosed area of $r(\theta)$, such that $\oint r^2(\theta) d\theta / 2 = A_r$. e_d is the shape factor of $r(\theta)$ and it measures the shape elongation of local void distribution. θ_d measures the principal orientation of $r(\theta)$. Figure 2 presents $r(\theta)$ of particle-void cells with different magnitude of e_d , ranging from 0.01 to 0.30 (Wei and Zhang 2020). With the increase

of e_d , the cell becomes elongated and local void distribution around the central particle is non-uniform. Furthermore, relative large pores can be observed besides the particle with a higher value of e_d .

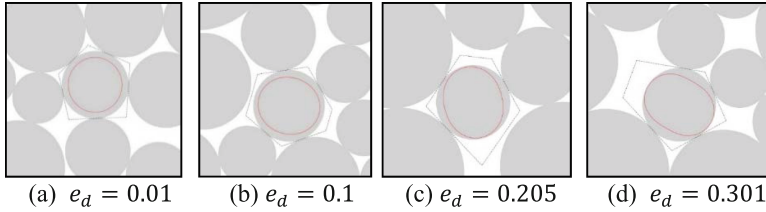


Fig. 2. $r(\theta)$ of particle-void cells with different magnitude of e_d , ranging from 0.01 to 0.3 (from Wei and Zhang 2020).

In the approach, particle-void descriptors (denoted as E_d and A_d) are derived from statistical analysis of e_d and θ_d to quantify void-based fabric of the whole packing. E_d is defined as the mean value of e_d of all cells, and it measures the shape elongation of the local void distribution throughout the packing. A_d is defined to quantify the anisotropy degree of particle-void fabric. E_d and A_d have a strong correlation with cyclic mobility and jamming transition in post-liquefaction stage of granular soils (Wei et al. 2018).

Figure 3 presents the initial value of E_d for samples with $p_0 = 10$ kPa.m before any shearing. A linear function can be employed to describe the relationship between E_d and void ratio e :

$$E_d = ke + T \tag{7}$$

where k is scale factor and T is intercept. The scale factor k is determined by particle size distribution of granular packing. In this study, the value of k is around 0.55.

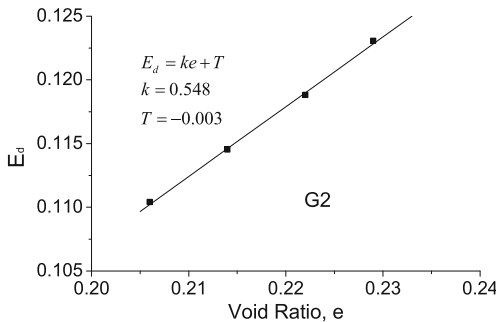


Fig. 3. The initial value of E_d for samples with different void ratio under confining stress $p_0 = 10$ kPa.m.

3 Results and Observations

3.1 Cyclic Liquefaction

To explore the characteristics of particle-void fabric for granular packing with different confining stresses, all samples are subjected to the undrained cyclic loading tests, in which the volume of the packing is kept constant and the decrease of mean effective stress can be observed. Figure 4 demonstrates representative results from sample with $e = 0.214$ during the loading test with axial strain amplitude $\varepsilon_a = 0.5\%$. The simulation results are qualitatively similar to laboratory results of medium-dense sands (Figueroa et al. 1994). With the increase of cycle number, both the amplitude of deviatoric stress q and mean effective stress p' decrease. The loading is terminated when the packing reaches initial liquefaction, in which the mean effective stress p' is close to zero and coordination number Z is lower than 2. As shown in Fig. 4(c) and (d), sample reaches the initial liquefaction after 25 loading cycles, as p' decreases from initial value of 10 kPa·m to 10^{-3} kPa·m and Z decreases from initial value of 3.67 to 1.89.

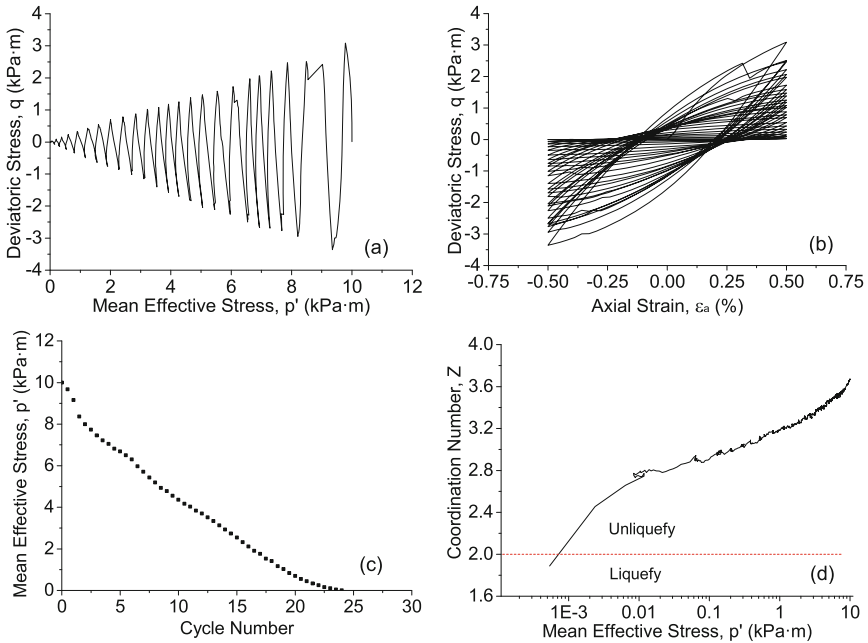


Fig. 4. Responses of sample with $e = 0.214$ during undrained cyclic loading test with axial strain amplitude $\varepsilon_a = 0.5\%$. (a) Effective stress path; (b) Evolution of deviatoric stress q with axial strain ε_a ; (c) Decrease of mean effective stress p' with the increase of cycle number; (d) Evolution of Z with the decrease of p' .

We further check the evolution of particle-void descriptors E_d and A_d during the cyclic liquefaction process and the results are presented in Fig. 5. To get rid of the influence of shear-induced anisotropy, the data of E_d , A_d and p' in Fig. 5 are picked

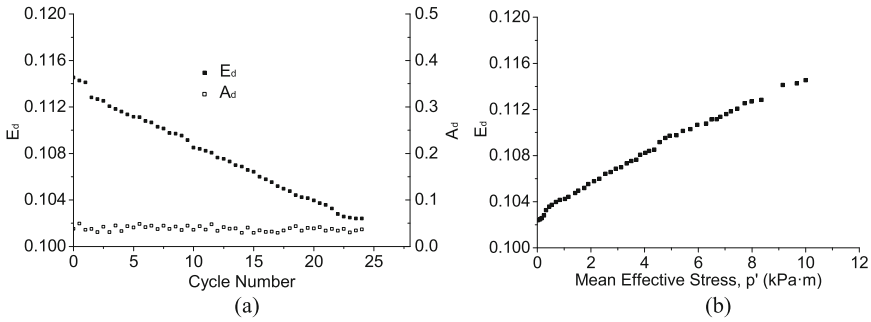


Fig. 5. Typical response of particle-void fabric evolution during cyclic liquefaction process for sample with $e = 0.214$. (a) Evolution of E_d and A_d with the increase of cycle number; (b) Evolution of E_d versus p' .

at zero deviatoric stress state (i.e. $q = 0$) in each loading cycle. With the increase of cycle number, the value of A_d remains at a relative low range during the whole loading process. It implies that the void-based fabric at zero deviatoric stress state can be regarded to be isotropic. On the other hand, E_d decreases from the initial value of 0.114 to 0.102. Figure 5(b) demonstrates the evolution of E_d versus p' during cyclic liquefaction process. A positive correlation between p' and E_d can be observed. Similar behaviors are also found in the monotonic loading tests (Wei and Zhang 2020).

3.2 E_d with P'

The evolution of E_d in accompany with the decrease of p' for samples with different particle size distributions and void ratios are presented in Fig. 6(a). For all samples, a positive correlation between E_d and p' can be observed, and the slope of the curve gradually increase with the decrease of p' . It is interesting to find that the curves for different samples are almost paralleled with each other. The results imply that the change of particle-void fabric during the entire cyclic liquefaction process may be irrelevant to void ratio of the sample. The insets of the figure further present ΔE_d for samples from consolidated state $p' = 10$ kPa·m to initial liquefaction state. The value of ΔE_d for samples with different void ratios are close to each other, which is -0.0122 .

Considering the linear relationship between E_d and void ratio e at consolidated state with $p' = 10$ kPa·m (refers to Eq. 7), the value of E_d at initial liquefaction state (denoted as $E_{d,0}$) is also linearly related with void ratio:

$$E_{d,0} = E_d + \Delta E_d = ke + T_0 \tag{8}$$

Note that $E_{d,0}$ can be regarded as the minimum value of E_d for the packing in the pre-liquefaction stage. After initial liquefaction, E_d will keep decreasing with continued cyclic loading (Wei et al. 2018).

The relationship between E_d and p' can be well fitted by a power function:

$$E_d = a(p')^b + E_{d,0} \tag{9}$$

where a and b are fitting parameters. Combining the linear correlation between $E_{d,0}$ and e in Eq. (8), we can get the following equation to predict E_d from p' and e of the granular packing:

$$E_d = a(p')^b + ke + T_0 \tag{10}$$

Figure 6(b) presents the curve fitting by Eq. (10). The parameters in the equation are summaries below: $a = 2.44 \times 10^{-3}$, $b = 0.70$, $k = 0.548$ and $T_0 = -0.015$.

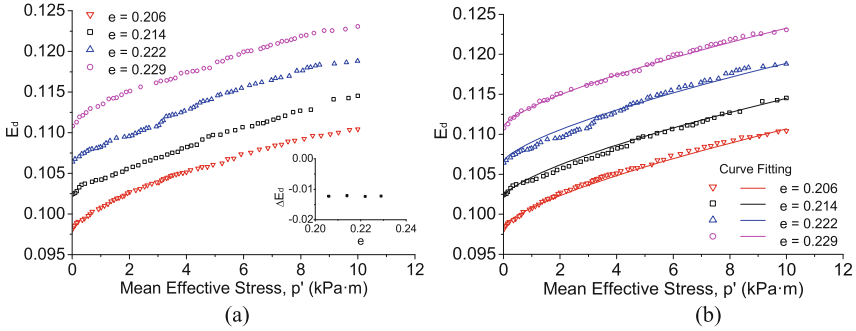


Fig. 6. Evolution of particle-void fabric indicator E_d in accompany with p' for samples with different void ratios.

4 Conclusions

In summary, the relationship between void-based fabric and mean effective stress p' during cyclic liquefaction process is explored by DEM simulations. Void-based fabric is quantified by particle-void descriptor E_d , which measures the uniformity of local void distribution around particles. Under the same confining pressure, a linear function can be employed to describe the positive correlation between E_d and void ratio e . With the decrease of p' during cyclic liquefaction process, the decrease of E_d is observed for all samples with different void ratios. From consolidated state ($p' = 10$ kPa·m) to initial liquefaction state, the change of E_d is almost the same for samples with different void ratios, which implies that the change of void-based fabric during cyclic liquefaction process is irrelevant to density of the packing. A power function is further adopted to describe the negative correlation between E_d and p' .

Acknowledgements. This research was supported by the National Natural Science Foundation of China (51908471). The financial supports are gratefully acknowledged.

References

Bowman, E.T., Soga, K., Drummond, W.: Particle shape characterisation using Fourier descriptor analysis. *Geotechnique* **51**(6), 545–554 (2001)

- Christoffersen, J., Mehrabadi, M.M., Nemat-Nasser, S.: A micromechanical description of granular material behavior. *J. Appl. Mech.* **48**(2), 339–344 (1981)
- Figuroa, J.L., Saada, A.S., Liang, L., Dahisaria, N.M.: Evaluation of soil liquefaction by energy principles. *J. Geotech. Eng.* **120**(9), 1554–1569 (1994)
- Gu, X., Yang, J., Huang, M.: DEM simulations of the small strain stiffness of granular soils: effect of stress ratio. *Granular Matter* **15**(3), 287–298 (2013)
- Ghedra, R., O'Sullivan, C.: Quantifying void fabric using a scan-line approach. *Comput. Geotech.* **41**, 1–12 (2012)
- Huang, X., Kwok, C.-Y., Hanley, K.J., Zhang, Z.: DEM analysis of the onset of flow deformation of sands: linking monotonic and cyclic undrained behaviours. *Acta Geotech.* **13**(5), 1061–1074 (2018). <https://doi.org/10.1007/s11440-018-0664-3>
- Idriss, I., Boulanger, R.: *Soil Liquefaction During Earthquakes*. Earthquake Engineering Research Institute, Oakland, California (2008)
- Li, X., Li, X.S.: Micro-macro quantification of the internal structure of granular materials. *J. Eng. Mech.* **135**(7), 641–656 (2009)
- O'Sullivan, C.: *Particle-based Discrete Element Modeling: A Geomechanics Perspective*. Taylor & Francis, Hoboken (2011)
- Seguin, A.: Experimental study of some properties of the strong and weak force networks in a jammed granular medium. *Granular Matter* **22**(2), 1–8 (2020). <https://doi.org/10.1007/s10035-020-01015-z>
- Shamoto, Y., Zhang, J., Goto, S.: Mechanism of large post-liquefaction deformation in saturated sand. *Soils Found.* **37**(2), 71–80 (1997)
- Sitharam, T.G., Vinod, J.S., Ravishankar, B.V.: Post-liquefaction undrained monotonic behaviour of sands: experiments and DEM simulations. *Géotechnique* **59**(9), 739–749 (2009)
- Šmilauer, V., Catalano, E., Chareyre, B.: *Yade Documentation*, 2nd edn. The Yade Project (2015)
- Vaid, Y., Stedman, J., Sivathayalan, S.: Confining stress and static shear effects in cyclic liquefaction. *Can. Geotech. J.* **38**(3), 580–591 (2001)
- Wang, G., Wei, J.: Microstructure evolution of granular soils in cyclic mobility and post-liquefaction process. *Granular Matter* **18**(3), 1–13 (2016). <https://doi.org/10.1007/s10035-016-0621-5>
- Wang, R., Fu, P., Zhang, J.-M., Dafalias, Y.F.: DEM study of fabric features governing undrained post-liquefaction shear deformation of sand. *Acta Geotech.* **11**(6), 1321–1337 (2016). <https://doi.org/10.1007/s11440-016-0499-8>
- Wei, J., Huang, D., Wang, G.: Microscale descriptors for particle-void distribution and jamming transition in pre-and post-liquefaction of granular soils. *J. Eng. Mech.* **144**(8), 04018067 (2018)
- Wei, J., Zhang, Y.: The relationship between contact-based and void-based fabrics of granular media. *Comput. Geotech.* **125**, 103677 (2020)
- Yang, J., Sze, H.: Cyclic behaviour and resistance of saturated sand under non-symmetrical loading conditions. *Géotechnique* **61**(1), 59–73 (2011)
- Yimsiri, S., Soga, K.: DEM analysis of soil fabric effects on behaviour of sand. *Géotechnique* **60**(6), 483–495 (2010)
- Zhang, J., Majmudar, T.S., Tordesillas, A., Behringer, R.P.: Statistical properties of a 2D granular material subjected to cyclic shear. *Granular Matter* **12**(2), 159–172 (2010)